Preprints of the 21st IFAC World Congress (Virtual)
Berlin, Germany, July 12-17, 2020

An Approach to Magnetometer-free On-body Inertial Sensors Network Alignment

Michael Lorenz * **Bertram Taetz** * **Gabriele Bleser** *

* *Technische Universiät Kaiserslautern, Kaiserslautern, Germany (e-mail: {surname}@cs.uni-kl.de).*

Abstract: To capture human motion with inertial sensors, they are attached as a network on different segments. Typically the measurements received from each sensor are fused to obtain its orientation. A challenging task is to align the orientation of each sensor w.r.t. to a single common coordinate frame. To fulfill this task typically the local magnetic field is measured to provide information about the heading direction. Since especially in indoor environments magnetic field disturbances can be present, this information is not a reliable source. To overcome this problem, we present a method that aligns an on-body inertial sensor network using gyroscopes and accelerometers only. The subject wearing the network had to fulfill a predefined procedure, consisting of standing still and walking straight. To extract the heading direction, we estimated the linear acceleration and angular velocity using a maximum-a-posteriori estimator. Performing a principal component analysis on the estimated states we computed two heading directions for each estimate. Instead of using them separately, we used a fusing approach that exploits symmetrical effects. We validated the approach on a lower body configuration using an optical motion capture system. The heading direction of sensors attached on a single leg could be aligned up to median maximal deviation of 2.6 degrees and on the complete lower body of 6.6 degrees. Especially deviations of the pelvis were higher, due to a lack of motion excitation. To be able to quantify the excitation needed, we proposed an indicator based on the ratio of the eigenvalues of the principal component analysis of the angular velocities.

Keywords: Human body motion capture, inertial sensors, sensor network, sensor alignment, spatial synchronization, motion estimation, information and sensor fusion, parameter and state estimation.

1. INTRODUCTION

The microelectromechanical systems (MEMS) technology allows to construct inertial measurement units (IMUs), also called inertial sensors, which are small, light-weighted and have a low power consumption. As Aminian and Najafi (2004) pointed out, this allows to attach them on the human body and apply them in numerous applications such as sports, rehabilitation or daily life monitoring. Usually MEMS IMUs are also equipped with a magnetometer, which allows them to measure the local magnetic field. Combining several IMUs in a sensor network attached to the human body, they are used in order to solve different tasks, like human body motion tracking or human motion analysis, as for instance done by Teufl et al. (2019), von Marcard et al. (2017) and Prathivadi et al. (2014). Usually such tasks are solved by first estimating the orientation of the moving body parts w.r.t. to a common coordinate frame (L), see Fig. 1. In a subsequent step the orientations are used to resolve the original problem. Regarding gold standard systems for human motion capturing, meaning optical motion capturing systems based on reflective markers, the primal task of obtaining the orientation w.r.t. to a reference coordinate frame is comparably simple. As shown in Guerra-Filho (2005), optical systems are able to capture the positions of markers w.r.t. to a local coordinate frame

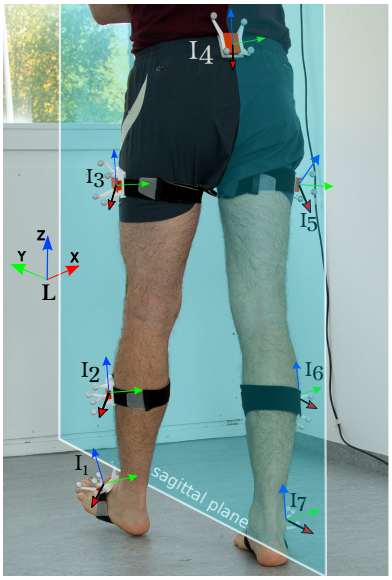

Fig. 1. The figure shows the experimental setup for the validation of our approach using seven IMUs and an optical motion capturing system. The common local coordinate frame (L) is used to orientate each IMU.

(L), see Fig. 1. Assuming that minimum three markers are attached rigidly on a body, also the orientation of the body can be computed w.r.t. to the local coordinate frame. Hence camera based systems capture all markers from the outside and then estimate the orientation w.r.t. to a local system. In contrast obtaining the orientation of each IMU is rather a challenging task when using inertial sensor network based systems. Each IMU of a network has to measure two different 3D vectors in its IMU coordinate frame. In addition the reference measurements in the local coordinate frame (L) have to be known. When both are given the measurements can be used to fuse the orientation of each sensor w.r.t. to the local coordinate system (L). The two 3D measurement vectors are typically obtained from different common measurable sources. One of the sources is typically gravity, which is measured by the accelerometer when the sensor is remaining still. With this the inclination of a sensor w.r.t. to gravity can be computed, see Kok et al. (2017). To know in which direction each sensor is heading, typically as a second source the local magnetic field measured by a magnetometer is used. For outdoor environments this might be a valid assumption. However, in indoor environments the magnetic field can be disturbed by ferromagnetic materials as shown by de Vries et al. (2009). Hence when initializing the orientation using measurements of the local magnetic field, the heading direction of each sensor might be corrupted.

There are magnetometer-free human motion tracking solutions, like Kok et al. (2014) or Taetz et al. (2016), which, however, need a single magnetometer measurement for each IMU to align the sensor network at the beginning of the tracking procedure. To get rid of this single measurement an alternative common source of the heading direction, which does not rely on the magnetic field, has to be introduced. In literature there exist several approaches of which only some can be used to align a inertial sensor network. All further mentioned solutions assume that the person carrying the sensors is walking straight for some time. Published work dealing with indoor positioning solutions uses mainly accelerometers to tackle related problems. Kunze et al. (2009) estimates the heading direction of a device in the trouser's pockets using a principle component analysis (PCA) on heuristically preprocessed raw accelerometer data. A similar approach to infer a heading direction for indoor navigation purposes is presented by, Hoseinitabatabaei et al. (2011), Kim et al. (2014) or Deng et al. (2015). It is an open question how well the latter approaches perform when aligning an inertial sensor network. There are also indoor positioning approaches which compute heading directions avoiding a PCA. For instance Nguyen et al. (2016) uses gyroscope and accelerometer measurements to compute the change of the heading direction of a single smartphone. However, since the change of the heading is considered, it is an open question whether this method is capable to align several IMUs in a network. The specific task of aligning an inertial sensor network is addressed in Xie et al. (2018). They show that it is possible to align five smartphones and a smart glass located at the upper part of the human body quite accurately. They use accelerometer signals when a person is moving to extract the heading direction using a PCA. Additionally gyroscope data is only used in an orientation tracking procedure. Recently Nazarahari and Rouhani (2019) applied a gyroscope-based solution to the field of biomechanics. To obtain the sensor-to-body calibration of inertial sensors attached to lower limbs the common heading information is extracted using the gyroscope measurements. Here a PCA on gyroscope measurements is used to obtain information about the heading.

The novelty of this work is a method which estimates a heading direction for each sensor of the network w.r.t. to a local coordinate system exploiting symmetrical effects between angular velocities and accelerations when a person is walking straight. Using additionally information about the inclination of each sensor w.r.t. to gravity the on-body inertial sensor network can be aligned. In a first step angular velocities and linear accelerations of each sensor are estimated using a Bayesian smoothing approach. Performing a PCA on each estimate we are able to extract two directions from each estimate. The two heading directions from angular velocity and linear acceleration are fused to a common heading direction exploiting symmetries between them. Experimental results show that the combined heading estimate outperforms the ones obtained using acceleration or angular velocity only as done in previous works. Also we propose an indicator to detect, when a body part/segment underwent sufficient movement to extract the heading direction. The approach is validated on a lower body configuration with an optical motion capture system.

The work is structured as follows: After the approach of extracting a common heading direction using gyroscope and accelerometer data is explained in Section 2, we evaluate it using an optical reference system in Section 3. For this we use a setup with seven IMUs fixed in casings equipped with four reflective markers attached to the lower body as illustrated in Fig. 1. Based on the results of the evaluation, Section 4 presents a critical discussion of the performance. The work is completed by conclusions and possible future work in Section 5.

2. METHOD

Our approach to find a common heading direction given an on-body inertial sensor network requires the fulfillment of a pre-defined procedure. This procedure is schematically summarized in Fig. 2 by the white boxes. First, the person has to stand still for about a second. In this period the inclination of each sensor w.r.t. to gravity is computed. In a second step the person has to walk for some steps into a predefined direction. To have enough excitation to extract a common heading direction, we assumed a minimum of three steps. Given the measurements we extracted a common heading direction the following way: First we computed a maximum-a-posteriori (MAP) estimate of the linear acceleration a_t, angular velocity ω_t and orientation χ_t in a navigation frame associated to the sensor, which is explained in Section 2.1. Afterwards based on a PCA of the estimated states we extracted a common heading direction. This procedure is described in Section 2.2. Having a common heading direction in Section 2.3 the procedure of aligning the inertial sensors is described. The necessary computational steps are summarized by the colored boxes of Fig. 2.

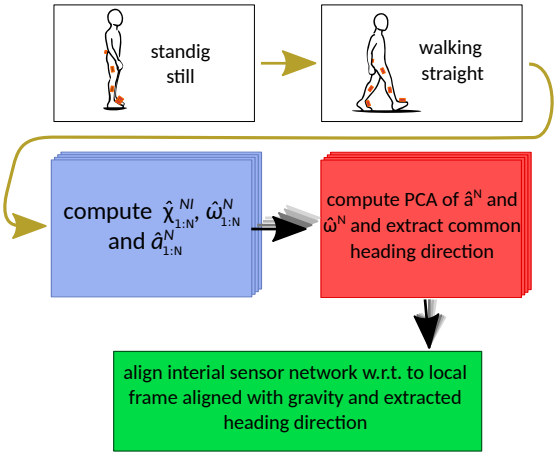

Fig. 2. Schematic description of the method to obtain a common heading direction for inertial sensor network alignment w.r.t. to a common local frame. The white boxes indicate the physical actions of the person. The colored boxes summarize the computational steps.

Before explaining the computational steps we introduce the needed coordinate frames. The coordinate frame of the ***i*th inertial sensor** I_i is aligned with the accelerometer triad and its coordinate axes are aligned with the casing of the sensor. Measurements obtained are given in this coordinate frames. The z-axis of the **local coordinate frame** L is aligned with gravity and the y-axis is aligned with the common heading direction extracted via the proposed method. These coordinate frames are illustrated in Fig. 1. In addition a **navigation coordinate frame** N_i associated to an inertial sensor i is needed. Like the local frame, its z-axis is also aligned with gravity but its y-axis is pointing into an arbitrary heading direction. A rotation matrix $R^{N_iI_i} \in \mathbb{R}^{3x3}$ rotates a three dimensional vector from the ith IMU coordinate frame to its navigation frame. The inverse rotation is given by

$$R^{I_iN_i} = \left[R^{N_iI_i}\right]^T \ . \tag{1}$$

2.1 Estimating the States

Instead of extracting a common heading direction from the raw sensor data directly, we used the gyroscope and accelerometer measurements in a sensor fusion approach to obtain the orientations and linear accelerations without gravity. This has the advantage that we were directly able to extract the estimated states in a plane orthogonal to gravity. Typical solutions use a Bayesian Filtering approach like an Extended Kalman Filter to obtain the estimated states. Its recursive nature allows fast computations. However, this is at the cost of a decreased accuracy. In contrast Bayesian Smoother approaches incorporate all information given a set of measurements and showed to be more robust in the presence of missing or corrupted data. In particular we computed a MAP estimate of the state trajectory for each sensor. As shown in Kok et al. (2017) the estimates obtained by such an estimator are more stable and accurate than the ones using an Extended Kalman Filter, especially when the sampling rates are low. Since an optimization problem has to be solved, this is achieved at the expense of an increased computational complexity.

The estimated states included orientation, linear acceleration and angular velocity. To represent orientations at a certain time t we made use of re-projected Modified Rodriguez Parameters (MRP) $\chi_t^{N_iI_i} \in \mathbb{R}^3$ as applied in Lorenz et al. (2019). In contrast to unit quaternions and their implied unity constraint, using this parametrization we avoided additional effort when solving the optimization problem (4). The linear acceleration of a sensor i in its navigation frame at time instance t is denoted by $a_t^{N_i} \in \mathbb{R}^3$. The angular velocity at time instance t was estimated in the IMU coordinate frame $\omega_t^{I_i} \in \mathbb{R}^3$. Its representation in the navigation frame was obtained by rotating it using the estimated orientations as

$$\omega_t^{N_i} = \mathbf{R}(\chi_t^{N_iI_i})\ \omega_t^{I_i} \ . \tag{2}$$

The rotation matrix with bold font $\mathbf{R}(\chi^{N_iI_i})$ denotes a conversion from MRPs to rotation matrices. Note that the states were estimated for each sensor individually in its navigation frame.

Assuming that N measurement samples contained the still-standing and walking phase the complete trajectory was estimated for a window of the same size. We therefore defined the vector of stacked states of time instance t as

$$x_t = [\ (\chi_t^{N_iI_i})^T\ (\omega_t^{I_i})^T\ (a_t^{N_i})^T\ ]^T \ . \tag{3}$$

With the assumption of Gaussian noise, the MAP estimator was analogously to Lorenz et al. (2019) formulated as the weighted nonlinear least square problem

$$\hat{x}_{1:N} = \underset{x_{1:N}}{\operatorname{argmin}} \underbrace{||e_1||^2_{P_1^{-1}}}_{\text{prior}} + \underbrace{\sum_{t=1}^{N} \left(||v_{a,t}||^2_{R_a^{-1}} + ||v_{\omega,t}||^2_{R_\omega^{-1}} \right)}_{\text{sensor measurements}} + \underbrace{\sum_{t=1}^{N-1} \left(||w_{\chi,t}||^2_{Q_\chi^{-1}} + ||w_{\omega,t}||^2_{Q_\omega^{-1}} + ||w_{a,t}||^2_{Q_a^{-1}} \right)}_{\text{dynamics}} \ . \tag{4}$$

Here $x_{1:N}$ indicates the stacked vector of the states of all time instances. The solution to the optimization problem is the estimate and is denoted as $\hat{x}_{1:N}$. The optimization problem (4) can be solved using standard methods like the Gauss-Newton or Levenberg-Marquardt method as explained in Nocedal and Wright (2006). Note, that the problem was solved for each sensor of the network individually. The terms of weighted sums are explained in the following.

Prior We assumed that the person is standing still for the beginning of the measurements for a predefined time. Although the human being is barely able to stand perfectly still, the accelerometer measurements showed only very low deviations from a static value. We defined that the acceleration measurements resulted only due to gravity. To account for small fluctuations we averaged the measurements for this period. Consequently we obtained an estimate of the gravity vector g^{I_i} for each sensor in its own IMU coordinate frame. We then defined an artificial heading direction measurement $\tilde{m}^{I_i} \in \mathbb{R}^3 : g^{I_i} \perp \tilde{m}^{I_i}$ pointing in arbitrary direction. It was computed applying the cross product as

$$\tilde{m}^{I_i} = g^{I_i} \times u \ , \tag{5}$$

where we defined the random vector $u \in \mathbb{R}^3 : u \neq k\, g^{I_i}$, and $k \in \mathbb{R}$. With $\tilde{m}^{I_i}$ and g^{I_i} we then computed the prior orientation $\bar{\chi}_1^{N_i I_i}$ w.r.t. to the navigation coordinate frame N_i using the triad method of Black (1964).
Since we assume that the sensor network is remaining still at the beginning the prior states on acceleration and angular velocity are zero. Having priors for the initial states the residual terms were computed as

$$e_1 = \begin{pmatrix} \bar{\chi}_1^{N_i I_i} - \chi_1^{N_i I_i} \\ \omega_1^{I_i} \\ a_1^{N_i} \end{pmatrix} , \tag{6}$$

where e_1 is assumed to be zero-mean Gaussian distributed with some known covariance matrix as $e_1 \sim \mathcal{N}(0, P_1)$.

Sensor Measurements Using the terms of the sensor measurements in (4), we extracted the estimated states from the measurements. We modeled these terms as

$$y_{a,t,i} = \mathbf{R}(\chi_t^{N_i I_i})^T (a_t^{N_i} - g^{N_i}) + v_{a,t} , \tag{7a}$$

$$y_{\omega,t,i} = \omega_t^{I_i} + v_{\omega,t} . \tag{7b}$$

Here $y_{a,t,i}$ indicates the accelerometer measurement and $y_{\omega,t,i}$ the gyroscope measurement at time instance t of sensor i. The gravity in the navigation frame, which is by definition the same as in the local coordinate frame, is given by g^{N_i}. The noises $v_{a,t}$ and $v_{\omega,t}$ are assumed to be Gaussian distributed as $v_{a,t} \sim \mathcal{N}(0, R_a)$ and $v_{\omega,t} \sim \mathcal{N}(0, R_\omega)$.

As Xing et al. (2017) pointed out, the effect of gyro-bias of MEMS IMUs does not have severe influence on estimates of short time considerations. Without loss of generality we omit the treatment of biases here and assume that the measurements are bias free or at least bias compensated. However, an inclusion of bias estimation is rather straightforward and can be found e.g. in Kok et al. (2017).

Dynamics Terms of the dynamics in (4) take care of the coupling between states of two consecutive time instances. Since the angular velocity is represented as rotation vectors and our orientation is estimated as re-projected MRPs we proceed the coupling over time by converting them to unit quaternions as

$$\mathbf{q}(\chi_{t+T}^{N_i I_i}) = \mathbf{q}(\chi_t^{N_i I_i}) \odot \mathbf{q}\left(T\left(\omega_t^{I_i} + w_{\chi,t}\right)\right) . \tag{8}$$

The conversions can be found in the work of Markley and Crassidis (2014) and are indicated by the $\mathbf{q}(\ )$ operator. The sampling interval is given by T. We assume the process noise to be $w_{\chi,t} \sim \mathcal{N}(0, Q_\chi)$. The dynamics of angular velocity and acceleration were modelled as random walk

$$\omega_{t+T}^{I_i} = \omega_t^{I_i} + w_{\omega,t} , \tag{9a}$$

$$a_{t+T}^{N_i} = a_t^{N_i} + w_{a,t} . \tag{9b}$$

Consequently the corresponding noises are modeled as $w_{\omega,t} \sim \mathcal{N}(0, Q_\omega)$ and $w_{a,t} \sim \mathcal{N}(0, Q_a)$.

2.2 Obtaining a common heading direction

Since for the alignment of the sensory network only a common heading direction is needed the components in direction of gravity were omitted. The z-component of linear acceleration in the navigation frame is dropped from here on. The angular velocities were estimated in the IMU coordinate frame. To obtain them in the associated navigation frame, they were rotated using the estimated orientations $\hat{\chi}_t^{N_i I_i}$ and applying (2). From here on the z-component of the angular velocity is also dropped. Given horizontal linear accelerations and angular velocities for each time instance we performed a PCA as described in Jolliffe (2002). The results of this procedure are illustrated in Fig. 3 for estimates of a left shank.

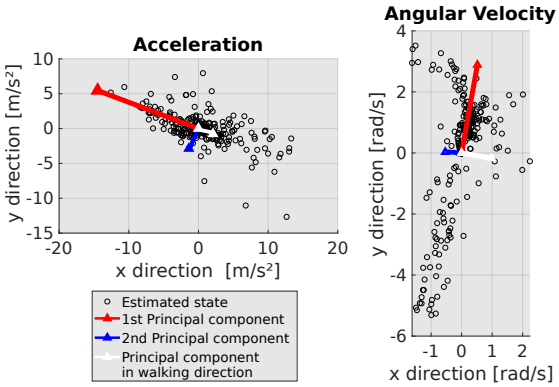

Fig. 3. Estimated values for horizontal linear acceleration and angular velocity in the navigation coordinate frame. The plots contain estimates of the still-standing period and three steps of an IMU attached on the left shank.

Rotations of the legs take mainly place in the sagittal plane, compare figure Fig. 1. Hence it can be assumed that the vectors of angular velocity are mainly parallel to the normal of the sagittal plane. The first principle component, shown as a red arrow in Fig. 3, reflects this behavior. For this reason the second principle component, which is orthogonal to the dominant component, is pointing in the direction of walking. Body parts which are not actively taking part in the bipedal walking locomotion such as the pelvis show the same behavior. However, for such body parts the first component was not as dominant as shown in Fig. 3. Since linear accelerations are acting in direction of walking one might assume that the first component is dominating the second. Hence the direction could be extracted from the first component. This might hold for the lower limbs. Pilot experiments showed that this assumption is not reliable for the pelvis. This is especially the case when the person starts to walk slowly and only low accelerations are acting in the horizontal plane. For this reason we assumed that the common heading obtained from the angular velocity only, $m_\omega^{N_i} \in \mathbb{R}^3 : ||m_\omega^{N_i}||_2 = 1$, was the second principle component of the horizontal angular velocity normalized to unity length. To obtain a heading direction from the linear acceleration, $m_a^{N_i} \in \mathbb{R}^3 : ||m_a^{N_i}||_2 = 1$, we computed dot products between the normalized principle components of the linear acceleration and $m_\omega^{N_i}$. The component with a closer value to ± 1 was selected as $m_a^{N_i}$.

Since principle components are ambiguous regarding their sense of direction, our computed directions are also ambiguous regarding their sign. To avoid this ambiguity we aligned $m_\omega^{N_i}$ and $m_a^{N_i}$ into direction of walking. To detect the forward direction, we used the same idea as done by Kourogi and Kurata (2003). When the person starts to walk during the time period $k \in [W_1, W_{\text{end}}]$ the low-pass filtered horizontal accelerations $\tilde{a}_{W_k}$ were pointing into

walking direction. Computing the dot product between the heading direction $m_a^{N_i}$ and $\tilde{a}_{W_1:W_{\text{end}}}$ it had to be

$$m_a^{N_i} \cdot \tilde{a}_{W_1:W_{\text{end}}}^{N_i} > 0 \,. \tag{10}$$

If (10) was negative, then $m_a^{N_i}$ had to be multiplied by -1. To obtain the right sense of direction for $m_\omega^{N_i}$ the same procedure using $m_a^{N_i}$ was applied. Therefore the equation

$$m_\omega^{N_i} \cdot m_a^{N_i} > 0 \,, \tag{11}$$

had to be fulfilled if the sense of direction was correct.

To understand the idea behind a heading direction which was computed combining $m_\omega^{N_i}$ and $m_a^{N_i}$, we make use of an exemplary result which is illustrated in Fig. 4. The graphic shows the estimated two individual heading directions for a lower body configuration. The mean values (green arrows) of the methods are pointing in a similar direction. However, in many cases directions of the segments were distributed symmetrically comparing $m_\omega^{N_i}$ and $m_a^{N_i}$. For instance the direction of the pelvis (black line) is on the right side of the mean for the case of linear acceleration and on the left side for the angular velocity. Both deviate about the same angle. To avoid these symmetrical deviations from the mean, we computed for every sensor i the combined common heading direction $m_c^{N_i} \in \mathbb{R}^3 : ||m_c^{N_i}||_2 = 1$ as

$$m_c^{N_i} = \frac{m_\omega^{N_i} + m_a^{N_i}}{||m_\omega^{N_i} + m_a^{N_i}||_2} \,. \tag{12}$$

The result of this procedure for this example is illustrated in Fig. 5.

2.3 Aligning the sensors to a common coordinate frame

Having an estimate of a common heading direction, each sensor was aligned from its associated navigation coordinate frame to a common local coordinate frame (L). Therefore each sensor's individual estimate of the common heading direction $m_c^{N_i}$ was rotated into its IMU coordinate frame to obtain $m_c^{I_i}$, using the inverse operation of (2). Consequently for each measurement of the IMU an additional measurement of a common heading direction is given in terms of the IMU coordinate frame. All inertial sensors of the network were aligned into one common local coordinate frame, using the triad method, as in Section 2.1.1.

2.4 Experimental setup

The presented approach was evaluated using a setup as depicted in Fig. 1.

Data Acquisition We captured the lower body using seven IMUs (MTW Awinda Xsens Technologies BV, Enschede, The Netherlands). They were rigidly set into a custom 3D printed casing with four reflective markers. The casing and IMUs were attached on the pelvis, thighs, shanks and feet using elastic stripes. An optical motion capture system (13 OptiTrack Prime Cameras NaturalPoint Inc. Corvallis, OR, USA) was used to track the reflective markers of the casing. Both systems were hardware synchronized using a standard 5V transistor-transistor-logic signal. We recorded data at a sampling frequency of 60 Hz. The alignment between the IMU coordinate frames

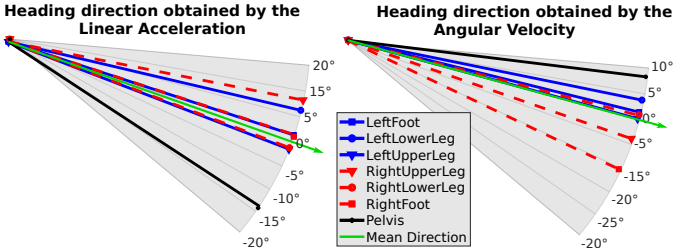

Fig. 4. Estimated common heading directions of acceleration only and angular velocity only. The plot shows the direction in the local frame for each segment of the lower body. The resulting directions were compared using an optical reference system as described in Section 3.

and the optical reference system (hand eye) was computed using the measured angular velocities as done by de Vries et al. (2009). The bias of the gyroscopes was estimated in a calibration procedure as done by Kok et al. (2017). The gyroscopes measurements were then compensated by the estimated bias.

Subjects and motions Thirteen healthy subjects (eight female and five male) were asked to stand still for about a second and then walk straight at a self-chosen speed. A trajectory of $N = 330$ samples was smoothed to obtain the estimated states. During this period the persons made three to seven steps. Two persons were walking with an approximate speed between $0.5m/s$ and $0.6m/s$. Three persons were walking with an approximate speed between $0.6m/s$ and $0.8m/s$. All other persons were walking with an approximate speed of $0.8m/s$ to $1.04m/s$.

Quantifying deviations When we initialize the the prior on the orientation $\bar{\chi}_1^{N_i I_i}$ as described in Section 2.1.1, each heading measurement $m_c^{N_i}$, $m_\omega^{N_i}$ and $m_a^{N_i}$ are obtained in its navigation coordinate system. Since they may be not perfectly aligned with each other, quantifying deviations among the senors is not possible. To evaluate the deviations we have to be able to compare the estimates in a pre-aligned coordinate system. For this reason the prior on the orientation $\bar{\chi}_1^{N_i I_i}$ of (6) was taken from the optical reference system for each sensor. Hence, all obtained estimates of the heading directions m^{N_i} were computed in the coordinate system of the optical motion capturing system. It was thus possible to compare the heading estimates with each other and to quantify the deviations among them.

3. EXPERIMENTAL RESULTS

Example results for one subject using the different methods are presented in Fig. 4 and Fig. 5. Except for one case all heading directions were pointing in a similar manner into direction of walking. We compared the deviations w.r.t. to a mean direction computed using all segments. The results are illustrated using box plots in Fig. 6. Recall that in a box plot the half of the values are given in the colored boxes and the other half is located in the region of the "antennas". The median values are illustrated as a red line in the box. The proposed combined approach outperformed the other solutions. The median values for the combined approach were on average closer to the mean direction. Also variances, which can be estimated

by the size of the boxes and antennas, were smaller and the robustness concerning outliers increased. Note, that the median values were nearly symmetrical distributed for the same segments of different sides. For instance was the median value m_c^L of the right foot was $-4.4°$ away from the mean and of the left foot was $3.1°$ away.

We also compared the maximal deviations from the mean direction w.r.t. different configurations of segments, which is illustrated in a box plot in Fig. 7. The values indicate how far the worst estimate was away from the mean direction. The deviations for single legs only were comparably low. For example was the median of maximal deviations for the combined approach at $2.6°$ for the right leg and at $2.4°$ for the left leg. The mean value for both legs was with $2.8°$ slightly higher than the median but in the same range. The single approaches performed with median values over $5°$ maximal deviation worse. Due to the symmetries mentioned before the maximal deviations for both legs increased. The combined approach yielded a median of $5.4°$. With the linear accelerations we achieved a value of $7.1°$ and with angular velocity $10.4°$. Aligning both legs

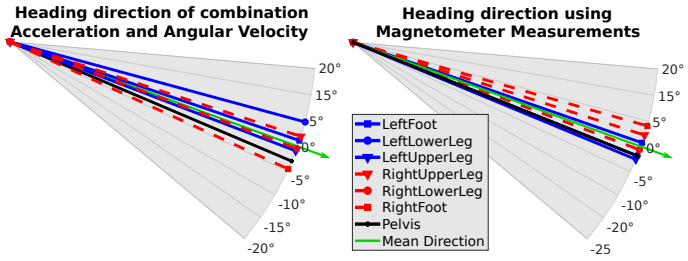

Fig. 5. Estimated common heading direction using the combined approach of acceleration and angular velocity (left plot). The right plot shows as a comparison the estimated heading direction using magnetometer measurements of the magnetic field. The meaning of the lines is the same as in Fig. 4.

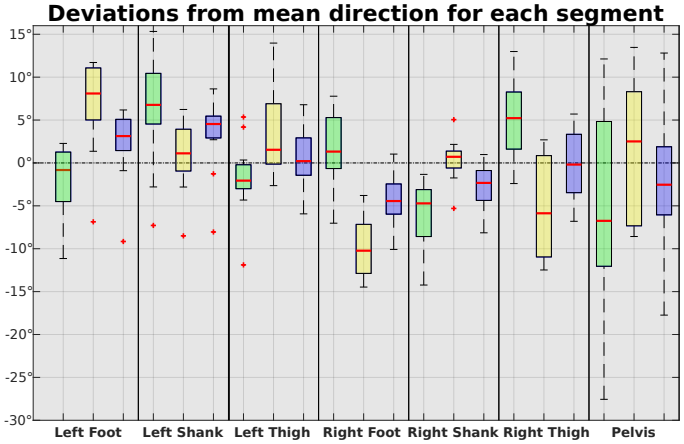

Fig. 6. The green boxes indicate the values using only acceleration m_a^L. The yellow boxes indicate the values using only angular velocity m_ω^L and the purple boxes indicate the values using the combined approach m_c^L. The thick red line in each colored box represents the median value for the direction. The dashed line at zero indicates the mean heading directions mean$(m_{a/\omega/c}^L)$ of the three different methods using all segments. The rot crosses outside the boxes represent the outliers.

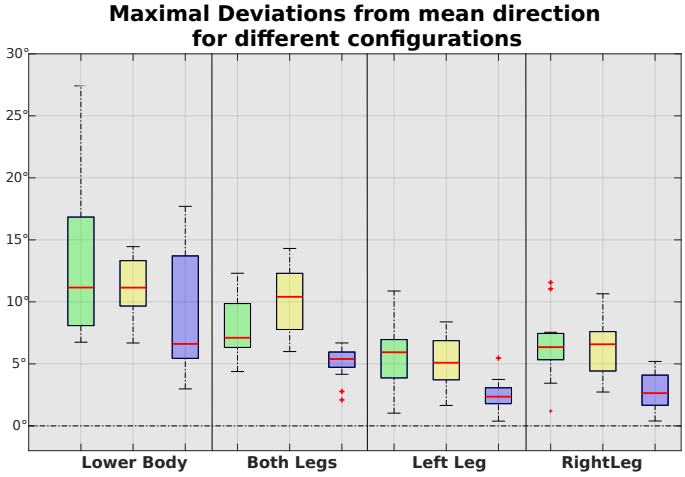

Fig. 7. The meaning of the boxes is the same as in Fig. 6.

only the spread of maximal deviations for the combined approach had a maximal value of $6.6°$ and a minimal value of $4.4°$, not including outliers. As illustrated in the column of the lower body in Fig. 7, adding the pelvis into consideration yielded poorer results. The maximal value for the maximal deviation reached $17.7°$ for the combined approach, not including the outlier. However, the minimal value for the maximal deviation is with $2.98°$ fairly low. Comparing the column for the pelvis in Fig. 6, it is clear that the significant increase of the variance for the lower body configuration is caused by the high variance of the estimates for the pelvis. Although the variance increased, considering the median value with $6.6°$ for the combined approach, it can be stated that it is only $0.8°$ worse than for median value of both legs. The mean value for a lower body configuration was at $12.0°$ fairly high. The significant difference to the median value is caused by an outlier.

In general legs exceeded enough excitation during walking. The difference between the estimates for persons who walked about $1.0m/s$ or slower than $0.8m/s$ was marginal. However, regarding the pelvis the amount of excitation significantly determined the quality of the heading estimate. The pelvis of four subjects did not perceive enough excitation to distinguish the walking direction. All four subjects were walking with small steps and managed to perform more than five steps. Two of them were walking less than $0.7m/s$ and two of them about $1.0m/s$. In these cases the estimated pelvis heading direction was corrupted by a lack of directional information. The ratio between the eigenvalues of the principle components of the angular velocity was smaller than two. In one particular case, where a female subject was walking five steps with a speed of $0.56m/s$ the ratio was at 1.2. Here the second principal component of the horizontal angular velocity was pointing orthogonal to the common heading direction. For this reason the forward direction could not be extracted from the second component as assumed in Section 2.2. This particular result of the pelvis is not visible in Fig. 6 and Fig. 7. They are marked as outliers beyond the scope of the plots. Also the principle components of the acceleration with the higher eigenvalues did not always point into direction of walking. For overall two cases the direction with the higher eigenvalue was also pointing orthogonal to the walking direction.

4. DISCUSSION

We showed that the introduced method is in general capable of aligning several inertial sensors in a network attached to the human body. Estimating the heading direction for a single leg performed with average value of 2.8° for the maximal deviation fairly well. However, if a common heading direction for all seven IMUs of the lower body was computed, the result was poorer. With an mean maximal deviation of 12.0° and median value of 6.6° for the lower body, it is an open question if such estimates are still valid to align an inertial sensor network in practice. The estimates of the lower body configuration suffer mainly from the heading estimate of the pelvis. For this body part it is important that enough excitation is present. The question how much excitation is needed remains still open. A suitable indicator might be the ratio of the eigenvalues of the angular velocity. For subjects having a ratio greater than two the estimated states had enough information to extract the heading direction using a PCA. However, this indicator only works under the assumption that the more excitation is present the higher are the amplitudes of angular velocity in the sagittal plane of the moving person. For this reason more investigations in this direction have to be undertaken.

During walking with a constant velocity the motion excitation of the pelvis is not that high as for example of the feet. A possibility to induce more excitation especially to the pelvis can be a different walking procedure. An example could be that the person first stands still, then walks for some steps straight and stands still again. Because of the additional stop some beneficial information might be induced, which could improve the results.

So far we computed the combined heading direction $m_c^{N_i}$ in (12) using a simple arithmetic mean. We performed also experiments on a version using a combination of the individual directions $m_\omega^{N_i}$ and $m_a^{N_i}$ weighted by the eigenvalues. However, since the magnitudes of the eigenvalues are of different orders it did not perform as well as the simple approach.

As de Vries et al. (2009) points out to avoid disturbances in the magnetic field a minimum distance of 100 cm to the irregularity causing materials should be preserved. Assuming that the main disturbances are caused by the ground one could apply a hybrid solution consisting of magnetometers and the proposed approach. Since aligning sensors on the legs performs fairly well, this could be used to align all sensors of the legs individually and then use the magnetic field to align other segments, which do not have enough excitation, with the upper legs. Here the ratio of the eigenvalues of the angular velocity can be used as a measure of excitation.

In literature the heading direction estimation just using a PCA on the linear accelerations is very common. However, in our experimental setup using just linear accelerations to extract the heading direction did not perform as well. This might be due to the fact that we also considered low walking velocities and hence low excitations.

5. CONCLUSIONS AND OUTLOOK

In this work we presented a method that enables an alignment of an inertial sensor network which is attached on the human body. From a predefined procedure, where the person has to stand still and then walk straight, we extracted a common heading direction. We therefore first estimated the linear accelerations and angular velocities for each sensor using a maximum-a-posteriori estimator. Applying a PCA on each estimate we computed two heading directions for one IMU. Instead of using these heading directions separately we exploited symmetrical effects to improve the heading estimate. We therefore computed a combined heading direction using the arithmetic mean. Given measures of gravity by the accelerometer and the combined heading direction the network could be aligned w.r.t. to a common local coordinate system.

We showed that the heading direction obtained by the combined approach outperforms an estimate using only linear acceleration or angular velocity. In particular considering each leg individually the heading direction could be extracted up to an average maximal deviation from the mean of 2.8°. The estimates of a common heading direction for all seven IMUs of the lower body were poorer with an average of 12.0° maximal deviation and a median of 6.6°. However, latter results origin from a lack of motion excitation in the pelvis segment. Evaluating the results we found that the ratio of the eigenvalues of the PCA can be used as indicator to determine whether enough motion excitation was present.

We plan to improve the combined estimate of the heading direction introducing a different walking procedure.

ACKNOWLEDGEMENTS

The project has received funding from the Federal Ministry of Education and Research under grant agreement No 16SV7115 and from the European Union's Horizon 2020 research and innovation programme under grant agreement No 779963 and 826304.

REFERENCES

Aminian, K. and Najafi, B. (2004). Capturing human motion using body-fixed sensors: Outdoor measurement and clinical applications. *Computer Animation and Virtual Worlds*, 15(2), 79–94. doi:10.1002/cav.2.

Black, H.D. (1964). A passive system for determining the attitude of a satellite. *AIAA Journal*, 2(7), 1350–1351. doi:10.2514/3.2555.

de Vries, W.H.K., Veeger, H.E.J., Baten, C.T.M., and van der Helm, F.C.T. (2009). Magnetic distortion in motion labs, implications for validating inertial magnetic sensors. *Gait & Posture*, 29(4), 535–541. doi: 10.1016/j.gaitpost.2008.12.004.

Deng, Z.A., Wang, G., Hu, Y., and Wu, D. (2015). Heading Estimation for Indoor Pedestrian Navigation Using a Smartphone in the Pocket. *Sensors*, 15(9), 21518–21536. doi:10.3390/s150921518.

Guerra-Filho, G.B. (2005). Optical motion capture: Theory and implementation. *Journal of Theoretical and Applied Informatics (RITA*, 12, 61–89.

Hoseinitabatabaei, S.A., Gluhak, A., and Tafazolli, R. (2011). uDirect: A novel approach for pervasive observation of user direction with mobile phones. In *2011 IEEE International Conference on Pervasive Computing and Communications (PerCom)*, 74–83. IEEE, Seattle, WA. doi:10.1109/PERCOM.2011.5767597.

Jolliffe, I.T. (2002). *Principal Component Analysis*. Springer Series in Statistics. Springer-Verlag, New York, 2 edition. doi:10.1007/b98835.

Kim, J.N., Ryu, M.H., Yang, Y.S., and Hong, J.Y. (2014). Estimation of Walking Direction Estimation using a Shoe-mounted Acceleration Sensor. *International Journal of Multimedia and Ubiquitous Engineering*, 9(5), 215–222. doi:10.14257/ijmue.2014.9.5.21.

Kok, M., Hol, J.D., and Schön, T.B. (2014). An optimization-based approach to human body motion capture using inertial sensors. *Proceedings of the 19th World Congress of the International Federation of Automatic Control (IFAC)*, 79–85.

Kok, M., Hol, J.D., and Schön, T.B. (2017). Using Inertial Sensors for Position and Orientation Estimation. *Foundations and Trends® in Signal Processing*, 11(1-2), 1–153. doi:10.1561/2000000094.

Kourogi, M. and Kurata, T. (2003). Personal positioning based on walking locomotion analysis with self-contained sensors and a wearable camera. In *The Second IEEE and ACM International Symposium on Mixed and Augmented Reality, 2003. Proceedings.*, 103–112. doi:10.1109/ISMAR.2003.1240693.

Kunze, K., Lukowicz, P., Partridge, K., and Begole, B. (2009). Which Way Am I Facing: Inferring Horizontal Device Orientation from an Accelerometer Signal. In *2009 International Symposium on Wearable Computers*, 149–150. IEEE, Linz, Austria. doi:10.1109/ISWC.2009.33.

Lorenz, M., Taetz, B., Kok, M., and Bleser, G. (2019). On Attitude Representations for Optimization-Based Bayesian Smoothing. In *Proceedings of the 22nd International Conference on Information Fusion*, 9. IEEE, Ottawa, Canada,.

Markley, F.L. and Crassidis, J.L. (2014). *Fundamentals of Spacecraft Attitude Determination and Control*. Number 33 in Space Technology Library. Springer, New York. OCLC: ocn882605422.

Nazarahari, M. and Rouhani, H. (2019). Semi-automatic Sensor-to-Body Calibration of Inertial Sensors on Lower Limb Using Gait Recording. *IEEE Sensors Journal*, 1–1. doi:10.1109/JSEN.2019.2939981.

Nguyen, P., Akiyama, T., Ohashi, H., Nakahara, G., Yamasaki, K., and Hikaru, S. (2016). User-friendly heading estimation for arbitrary smartphone orientations. In *2016 International Conference on Indoor Positioning and Indoor Navigation (IPIN)*, 1–7. IEEE, Alcala de Henares, Spain. doi:10.1109/IPIN.2016.7743642.

Nocedal, J. and Wright, S.J. (2006). *Numerical Optimization*. Springer Series in Operations Research. doi:10.1007/978-0-387-40065-5.

Prathivadi, Y., Wu, J., Bennett, T.R., and Jafari, R. (2014). Robust activity recognition using wearable IMU sensors. In *2014 IEEE SENSORS*, 486–489. doi:10.1109/ICSENS.2014.6985041.

Taetz, B., Bleser, G., and Miezal, M. (2016). Towards self-calibrating inertial body motion capture. In *Proceedings of the Information Fusion (Fusion), 2016 19th International Conference On*, 1751–1759. IEEE.

Teufl, W., Lorenz, M., Miezal, M., Taetz, B., Fröhlich, M., and Bleser, G. (2019). Towards Inertial Sensor Based Mobile Gait Analysis: Event-Detection and Spatio-Temporal Parameters. *Sensors*, 19(1), 38. doi:10.3390/s19010038.

von Marcard, T., Rosenhahn, B., Black, M.J., and Pons-Moll, G. (2017). Sparse Inertial Poser: Automatic 3D Human Pose Estimation from Sparse IMUs. *Computer Graphics Forum*, 36(2), 349–360. doi:10.1111/cgf.13131.

Xie, L., Cai, Q., Liu, A.X., Wang, W., Yin, Y., and Lu, S. (2018). Synchronize Inertial Readings From Multiple Mobile Devices in Spatial Dimension. *IEEE/ACM Transactions on Networking*, 26(5), 2146–2159. doi:10.1109/TNET.2018.2859246.

Xing, H., Hou, B., Lin, Z., and Guo, M. (2017). Modeling and Compensation of Random Drift of MEMS Gyroscopes Based on Least Squares Support Vector Machine Optimized by Chaotic Particle Swarm Optimization. *Sensors*, 17(10), 2335. doi:10.3390/s17102335.